IOPscience iopscience.iop.org

Home Search Collections Journals About Contact us My IOPscience

Morphology of nanodroplets on structured surfaces

This article has been downloaded from IOPscience. Please scroll down to see the full text article.

2013 J. Phys. D: Appl. Phys. 46 215302

(http://iopscience.iop.org/0022-3727/46/21/215302)

View the table of contents for this issue, or go to the journal homepage for more

Download details:
IP Address: 192.77.116.224
The article was downloaded on 13/05/2013 at 07:16

Please note that terms and conditions apply.

IOP PUBLISHING JOURNAL OF PHYSICS D: APPLIED PHYSICS

J. Phys. D: Appl. Phys. **46** (2013) 215302 (10pp) doi:10.1088/0022-3727/46/21/215302

Morphology of nanodroplets on structured surfaces

A Vahid and A Moosavi

Center of Excellence in Energy Conversion (CEEC), School of Mechanical Engineering, Sharif University of Technology, Azadi Avenue, PO Box 11365-9567 Tehran, Iran

E-mail: moosavi@sharif.edu

Received 13 December 2012, in final form 27 March 2013
Published 8 May 2013
Online at stacks.iop.org/JPhysD/46/215302

Abstract

We report different morphologies of nanodroplets over various topographical features of the supporting substrates. The effects of different parameters such as the profile of the disjoining pressure, droplet size and the geometrical parameters are studied and discussed. Also, the effects of a coating layer on the surface of the substrate are determined. It is demonstrated that the nanodroplets at some positions are not stable and gradually move to more stable positions so that the system has less energy. For grooves this results in a series of morphology diagrams of the nanodroplets over the grooves as a function of the grooves' width and the liquid volume.

(Some figures may appear in colour only in the online journal)

1. Introduction

The wetting behaviour of a liquid on a solid substrate is determined by the difference between the cohesive interactions holding the liquid together and the adhesive interactions between the liquid and the solid [1]. This is well known, and has found a variety of uses in different areas including in the chemical industry, automobile manufacturing, glass, food and soil science. It also plays a fundamental role in life science, for instance in the rise of sap in plants, adhesion of parasites on wet surfaces and wetting of the eye [2].

Generically, most solid surfaces are topographically (or chemically) heterogeneous. These disorders can have substantial effects on the wetting behaviour of these surfaces [3, 4]. Micro- and nanofluidics is another strong driving force for research on the dynamics of fluids on structured substrates. The wetting of the solid surfaces can be utilized to determine precisely defined routes based on the wetting gradients [5]. Similarly, we can use topographical surfaces for guiding liquids in micro- and nanofluidic devices [6–8]. Therefore, wetting phenomena on topographically structured substrates have been the subject of various research efforts using both the experimental and theoretical approaches [9]. However, despite various research performed on the topic, the studies are predominantly limited to either microscales or two-dimensional studies [10–16]. In [10–13] morphology of a liquid droplet clinging to a step edge, blob and channel which correspond to localized and delocalized morphological wetting states at the microscales has been studied. For the nanoscales phenomena the terms considered in the Young–Laplace relation are not sufficient to describe the behaviour of the system [17]. In [14, 15] the effects of different parameters on the final shape of nanodroplets over two-dimensional steps without considering the lateral dimension effects have been investigated numerically. Also, in [16] the morphology diagram for fluid dots in cylindrical holes for different holes, aspect ratios and filling degrees were obtained and the results were compared with the experimental outcomes. Good agreement between the results were found.

It is obvious that, for most of the cases, in order to have a thorough understanding of the behaviour of droplets on those scales a three-dimensional study is necessary. Therefore, in this study we solve mesoscopic hydrodynamic equations to study the morphology of the nanodroplets over topographically structured substrates. The effects of the intermolecular interactions can be considered in terms of the disjoining pressure (DJP) [18], $\Pi = -\partial\Phi(H)/\partial H$, where the so-called effective interface potential $\Phi(H)$ is the cost in free energy per unit area to maintain a wetting film of prescribed mean thickness H [6]. In contrast to homogeneous substrates where Π is independent of the lateral coordinates, parallel to the substrate surface, on topographically inhomogeneous substrates the DJP depends on the lateral coordinates. Since the lateral variation of the DJP can change the behaviour of droplets over topographically structured substrates, even qualitatively, we consider these lateral changes of the DJP in our study to determine morphology of the droplets [15]. We discuss the morphology of nanodroplets for three paradigmatic

 © 2013 IOP Publishing Ltd Printed in the UK & the USA

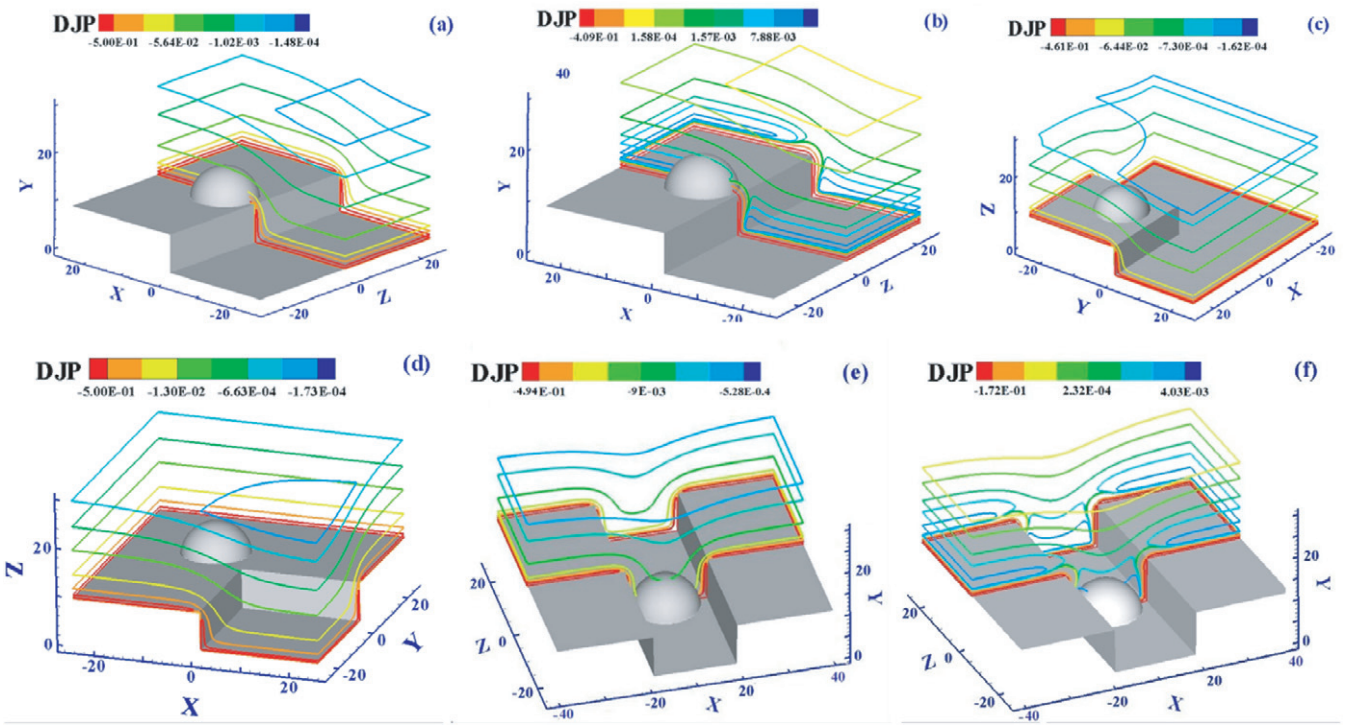

Figure 1. The distribution of the DJP over topographical features. The parameters of the DJP (B, C) in parts (a),(b),(c),(d),(e) and (f) are (2.667,0), (2.667,−2.5),(2.667,0), (2.667,0) and (1,−2.5), respectively. The lengths (x, y, z) and the DJP are measured in units of b and σ/b.

geometries. First, we start with a three-dimensional step, which is relatively a simple topography. Afterwards, we increase the complexity and investigate morphology of droplets on grooves and the behaviour of the system are specified for small liquid volume. Finally, the situation of the nanodroplets on three-dimensional edges and wedges will be studied. We assume that the fluids are Newtonian and nonvolatile, namely, the total volume of the fluid (in the film and the droplet) is considered fixed. We also suppose that the substrate is completely smooth and uniform in flat parts, namely, there is no roughness and chemical heterogeneity in these parts. Although this is not unrealistic [19], through this assumption we avoid many complexities in our study such as the hysteresis. We employ the sharp-kink model that assumes a step-like profile for the density [20]. The surface tension may depend on the curvature. Such complexities have been considered in terms of the DJP by correctly modelling the intermolecular interactions [21]. Since the type of the intermolecular interactions may be different the dependence on the curvature is not universal [21]. The densities of the liquid and the gas phases are considered to be equal to $1000\,\mathrm{kg\,m^{-3}}$ and $1\,\mathrm{kg\,m^{-3}}$, respectively. Also, the dynamic viscosities of the liquid and the gas phases are supposed to be $1e-6$ (Pa s) and $1.48e-5$ (Pa s), respectively. Changing these properties may clearly affect the dynamics of the system but since we are interested only in the final morphologies, considering different values for these properties will not change the results. The gas–liquid interface surface tension is assumed to be $0.07\,\mathrm{N\,m^{-1}}$. Changing this value will change both the dynamics and the equilibrium morphologies. However, since our results are presented based on dimensionless parameters and the surface tension effects are compared with the intermolecular forces, one can change the strength of the intermolecular forces instead of changing the surface tension. We also assume a no-slip boundary condition at the solid surface and neglect the influence of the thermal fluctuations [22]. The slip boundary condition can change the dynamics and is relevant at the nanoscales but considering no-slip boundary condition, again, does not change the results.

2. Methodology

The considered approach for studying the morphologies is essentially composed of two parts. The first part involves calculation of the DJP and the second part concerns the simulation of the flow field and deriving the equilibrium configuration of the gas–liquid interface.

2.1. Models of the heterogeneity

In the following, we describe the applied method for calculating the DJP over three-dimensional topographic edges, wedges and steps, as shown in figure 1. Considering that the fluid particles, as well as the fluid and the substrate particles, are taken to interact with each other via pair potentials $V_{\alpha\beta}$, where α and β refer to the phases, and also assuming additivity of the intermolecular interactions, the DJP is expressed as [14, 15]

$$\Pi = \int_{\Omega_s} \omega(\boldsymbol{r})\, \mathrm{d}^3\boldsymbol{r}, \tag{1}$$

where Ω_s is the volume of the solid(s) and r is the interatomic distance. $\omega(\boldsymbol{r})$, which corresponds to the local interaction

energy difference per unit volume squared between the solid and the vapour phase, is defined as [23]

$$\omega(\rho) = \rho_l^2 V_{ll}(\boldsymbol{r}) - \rho_l\rho_s V_{sl}(\boldsymbol{r}) - \rho_l\rho_v V_{lv}(\boldsymbol{r}) + \rho_v\rho_s V_{vs}(\boldsymbol{r}) \quad (2)$$

where the subscripts correspond to liquid (l), substrate (s) and vapour (v) (or another phase which is positioned above the liquid phase) and ρ is the particle number densities for each phase. By neglecting the vapour phase and considering a coating layer (c) on top of the substrates (s), one can show that the DJP of the system is given by

$$\Pi = \int_{\Omega_s} [\rho_l{}^2 V_{ll}(\boldsymbol{r} - \boldsymbol{r}') - \rho_l\rho_s V_{sl}(\boldsymbol{r} - \boldsymbol{r}')]\, \mathrm{d}^3\boldsymbol{r}. \quad (3)$$

In order to facilitate the calculation of the DJP for the three-dimensional topographical features we decompose them into contributions from the components. The contribution from the quarter spaces forming the body (Π_b) can be calculated either analytically or numerically. Since many substrates in the experiments, for modifying the wetting properties of the substrate, are coated, we assume that the surfaces are coated with a thin layer of a different material. The contributions from the thin coating layer (Π_c) can be considered similar to the main structure. Considering Lennard–Jones type pair potentials $V_{\alpha\beta}(\boldsymbol{r}) = M_{\alpha\beta}/r^{12} - N_{\alpha\beta}/r^6$ and substituting it in equation (3) leads to

$$\Pi_{b,c} = \int_{\Omega_s} \left[\frac{\Delta M_{b,c}}{|\boldsymbol{r} - \boldsymbol{r}'|^{12}} - \frac{\Delta N_{b,c}}{|\boldsymbol{r} - \boldsymbol{r}'|^6}\right] \mathrm{d}^3\boldsymbol{r}, \quad (4)$$

where $M_{\alpha\beta}$ and $N_{\alpha\beta}$ are material parameters, also $\Delta M_{b(c)} = \rho_l{}^2 M_{ll} - \rho_l\rho_{s(c)} M_{ls(lc)}$ and $\Delta N_{b(c)} = \rho_l{}^2 N_{ll} - \rho_l\rho_{s(c)} N_{ls(lc)}$. Ω_s is the volume of the body and the thin coating layer in the topographies. The first term dominates close to the surface of the edge and the second term dominates at large distances from the substrate.

In order to present the results in a dimensionless form, we write the lengths in units of $b = [2|\Delta M_b|/(15|\Delta N_b|)]^{1/6}$, which for $\Delta M_b > 0$ and $\Delta N_b > 0$ is the equilibrium wetting film thickness y_0 on the uncoated flat substrate [14, 15]. The DJP is scaled by σ/b where σ is the liquid-vapour surface tension. By considering these quantities and combining the contributions of the building blocks and also the thin coating layer with thickness d the DJP can be written as

$$\Pi^* = C\left[\int_{\Omega^*_{b\zeta}} \left(\frac{45}{\pi|\boldsymbol{r}^* - \boldsymbol{r}^{*\prime}|^{12}} - \frac{6}{\pi|\boldsymbol{r}^* - \boldsymbol{r}^{*\prime}|^6}\right) \mathrm{d}^3\boldsymbol{r}^* + B\int_{\Omega^{*\chi}_c} \left(\frac{2}{\pi|\boldsymbol{r}^* - \boldsymbol{r}^{*\prime}|^6}\right) \mathrm{d}^3\boldsymbol{r}^*\right], \quad (5)$$

where the asterisk symbol indicates that the relevant quantities are dimensionless. The subscript ζ refers to the type of the structure (edge, wedge, etc) and the superscript χ considers the sides which are coated. Hereinafter to avoid a clumsy notation we remove the star symbol. In this equation $C = [\pi b(|\Delta M_b|/45)^{-1/2}(|\Delta N_b|/6)^{3/2}]/\sigma$ determines the strength of the DJP relative to the surface tension and $B = [\pi\Delta N d]/[2b^4(|\Delta M_b|/45)^{-1/2}(|\Delta N_b|/6)^{3/2}]$ determines the strength of the coating layer. In equation (5) we have neglected the effects of the higher order terms in the coating layer [14]. For an equilibrium wetting with $b \neq 0$, $\Delta M_b \geqslant 0$ is necessary but ΔN_b can be either positive or negative. Corresponding to ΔN_b sign we refer to the DJP as the minus and the plus cases.

For the three-dimensional edge and wedge we solve the first and second terms of equation (5) numerically and then combine their contributions. Because of the semi-infinite intervals involved in the integrations ($\Omega_{be} = \{\boldsymbol{r} \in \boldsymbol{R} | x \leqslant 0 \wedge y \leqslant 0 \wedge z \leqslant 0\}$) we use the Gauss–Laguerre quadrature method for calculating these integrals. For the three-dimensional step the procedure is similar to other geometries, but in this case integrals of equation (5) can be calculated analytically. Since detailed descriptions for calculating the DJP are given in [15], we just mention the final expression for a coated step or a two-dimensional coated edge ($\Omega_{ce} = \{\boldsymbol{r} \in \boldsymbol{R} | x \leqslant 0 \wedge y \leqslant 0\}$). In dimensionless form the DJP is given as

$$\Pi_{ce}(x, y) = \Pi_{be}(x + b, y + b) + \Pi^u_c(x, y) + \Pi^r_c(x, y) \quad (6)$$

where $\Pi^u_c(x, y)$ and $\Pi^r_c(x, y)$ refer to the DJP contributions from the coating layers placed on the upper side (u) and the right part (r) of the edge. Due to the symmetry of the geometry, the DJP of upper side of the edge $\Pi^u_c(x, y)$ is equal to $\Pi^r_c(y, x)$ in the right side of the edge. Π^u_c and Π_{be} are given as:

$$\Pi^u_c(x, y) = \frac{b}{256y^{10}(x^2 + y^2)^{9/2}}[128(x^2 + y^2)^{9/2} - 315xy^8 - 840x^3y^6 - 1008x^5y^4 - 576x^7y^2 - 128x^9] + \frac{b}{4y^4(x^2 + y^2)^{3/2}}[-2(x^2 + y^2)^{3/2} + 3xy^2 + 2x^3], \quad (7)$$

$$\Pi_{be}(x, y) = \frac{1}{256x^9y^9(x^2 + y^2)^{7/2}}[-280x^6y^6(x^4 + y^4) - 448x^2y^2(x^{12} + y^{12}) - 128(x^{16} + y^{16}) - 35x^8y^8 + 128(x^9 + y^9)(x^2 + y^2)^{7/2} - 560x^4y^4(x^8 + y^8)] + \frac{1}{4x^3y^3(x^2] + y^2)^{1/2}}[2(x^3 + y^3)(x^2 + y^2)^{1/2} - 2(x^4 + y^4) - x^2y^2]. \quad (8)$$

Using the superposition and combining the DJP for two quarters, the final form of the DJP for the three-dimensional step is

$$\Pi(x, y) = \Pi_{ce}(x, y + h) + \Pi_{ce}(-x, y) - 2\Pi^r_c(x, y) \quad (9)$$

where h is height of the step. In a similar way, by adding all the contributions, the DJP in a groove with a rectangular cross section can be given as

$$\Pi(x, y) = \Pi_{Be}(x, y + h) + \Pi_{Be}(-x, y) - 2\Pi^r_{Ce}(x, y) - \Pi_{Be}(-x + w, y) + \Pi_{Be}(-(x + w), y + h) - 2\Pi^r_{Ce}(-(x + w), y), \quad (10)$$

where w represents the width and h is the height of channel. The distribution of the resulted DJP is depicted in figure 1.

We derive the DJP in a flat substrate far from heterogeneities which can be derived by considering $h = 0$ in equation (9) as

$$\Pi_{ch}(y) = C\left[\left(\frac{1}{y^9} \mp \frac{1}{y^3}\right) + \frac{B}{y^4}\right]. \quad (11)$$

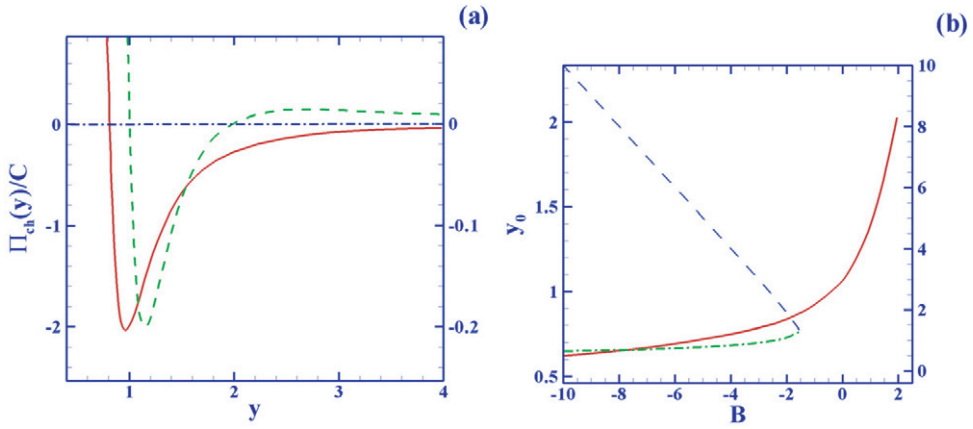

Figure 2. (*a*) A typical profile of the DJP for both the plus(dashed lines) and the minus(full lines) case over a flat homogeneous substrate corresponding to ($B = -2$) and in units of C; The right vertical axis belongs to the dashed line and the left axis is for fulled line. Part (*b*) displays zero values of the DJP for different values of B for both the minus (full line) and the plus (dashed and dotted–dashed lines) cases. Full and dotted–dashed lines represent stable wetting films and dashed line shows an unstable situation.

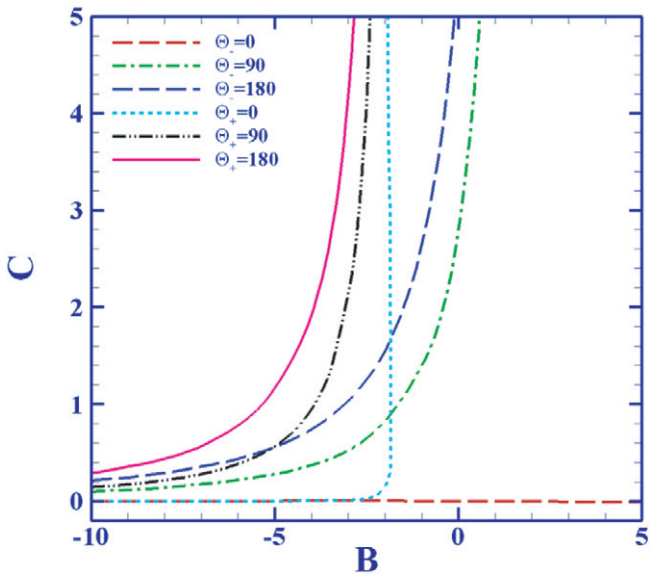

Figure 3. Allowable values of θ_{eq} for the plus (θ_+) and the minus (θ_-) cases. According to the figure, θ_{eq} should be in the range of $0^\circ \leqslant \theta_{eq} \leqslant 180^\circ$.

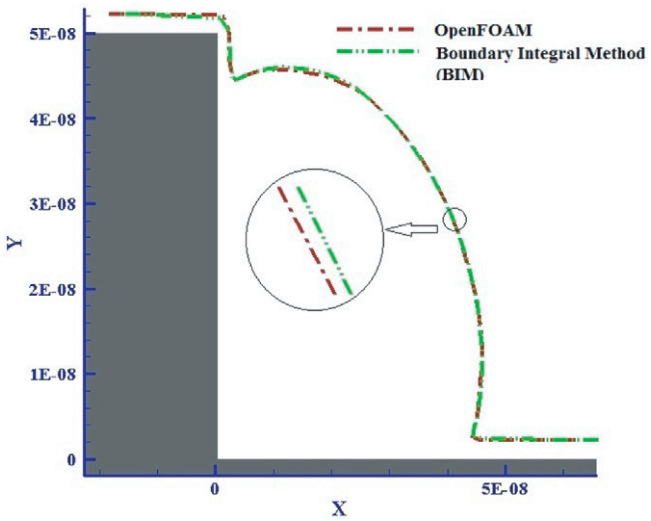

Figure 4. A comparison between the final shape of a droplet positioned on a step with $h = 5$, obtained from the present numerical algorithm and the boundary integral method [15]. The area of the droplet is equal to 250 and the DJP profile belong to the plus case with the parameters $B = -2.5$ and $C = 6$, corresponding to $\theta_{eq} = 114.7^\circ$.

Values of B and C can be adjusted for arbitrary contact angles from

$$\cos\theta = 1 + \int_{y_0}^{\infty} \Pi_{ch}(y)\,dy, \tag{12}$$

where the size of y_0, which is the wetting film thickness for zero DJP, is derived from

$$\frac{1}{y_0^9} \mp \frac{1}{y_0^3} + \frac{B}{y_0^4} = 0. \tag{13}$$

Figure 2 shows the typical profile of the DJP for both the minus and the plus cases. Also, figure 3 displays the allowable values of B and C.

2.2. *Governing equations and the numerical method*

From one perspective, two main approaches for calculating free surface flow problems can be identified. In the first approach one uses a dynamic mesh and the boundaries of the grid form the gas–liquid and other interfaces but in the second method the interface is moved through a fixed grid. In this study, we apply a volume of fluid (VOF) based routine which is basically a fixed-grid method. The VOF method is based on solving the Navier–Stokes equations together with an equation for the volume fraction function α value of which is unity at any point occupied by fluid and is zero otherwise. It should be noted that for deriving the morphologies it is not necessary to solve the hydrodynamic equations and an approach to determine the configuration of the system for which the energy of the system is minimum is adequate [16]. However, since the behaviour of the system is ultimately determined by study of the dynamics and in the future studies our goal is to consider the dynamics, in order to apply a unique method for both the investigations, we also study the stationary situations via solving the hydrodynamic equations.

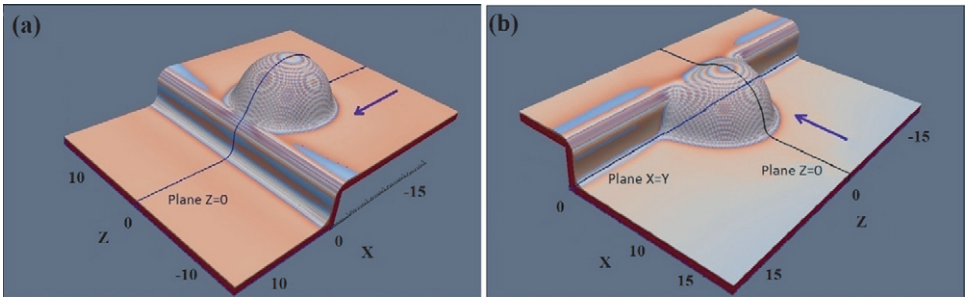

Figure 5. Droplets positioned on the top and the bottom sides of the step move toward the edge and the wedge regions, respectively, for the minus case of the DJP. The selected planes ($z = 0$, $x = y$) are used in the following figures.

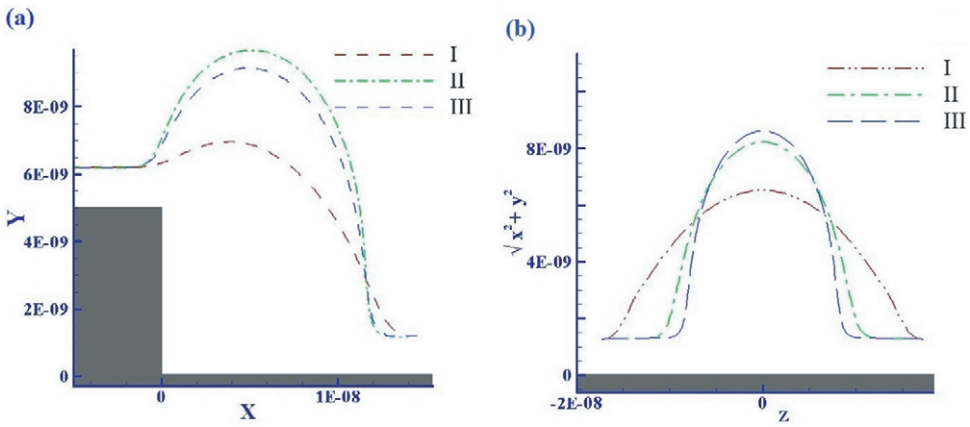

Figure 6. The effect of the DJP profile (B, C) on the configuration of the droplets positioned on the bottom side of the step. The values of B and C are I ($B = 0$, $C = 1.5$), II ($B = 0$, $C = 3$) and III ($B = 0$, $C = 3.5$). The height of the step is equal to $h = 5$ and for all the cases the volume of the liquid is the same. The parts (a) and (b) display $z = 0$ and $x = y$ planes (see part (b) of figure 5).

The interface is reconstructed from the α field. Particularly, a unit value of α would correspond to a cell full of fluid, while a zero value would indicate that the cell contains no fluid. Cells with α values between zero and one ($0 < \alpha < 1$) contain the free surface [24].

$$\alpha = \begin{cases} 1 & \text{if there is a liquid cell ,} \\ 0 < \alpha < 1 & \text{if there is a two-phase cell,} \\ 0 & \text{if there is a gas cell.} \end{cases}$$

First, we solve the momentum and the continuity equations for an incompressible Newtonian fluid for entire computational domain, given by

$$\nabla \cdot \boldsymbol{U} = 0, \tag{14}$$

$$\frac{\partial(\rho(\alpha)\boldsymbol{U})}{\partial t} + \nabla \cdot (\rho(\alpha)\boldsymbol{U} \otimes \boldsymbol{U}) - \nabla \cdot (\mu(\alpha)\nabla \boldsymbol{U}) = -\nabla P + \rho(\alpha)\boldsymbol{g} + \boldsymbol{F}_{\mathrm{s}}. \tag{15}$$

where $\boldsymbol{U}$ represents the velocity vector, P is the pressure, t stands for the time, ρ is the fluid density, μ denotes the fluid viscosity, $\boldsymbol{g}$ is the gravitational acceleration and $\boldsymbol{F}_{\mathrm{s}}$ stands for the normal forces acting on the liquid surface.

The physical properties of the fluid are calculated based on the volume fraction of the two fluids in one cell. The density $\rho(\alpha)$ and the dynamic viscosity $\mu(\alpha)$ can be written as

$$\rho(\alpha) = \alpha\rho_{\mathrm{l}} + (1 - \alpha)\rho_{\mathrm{g}}, \tag{16}$$

$$\mu(\alpha) = \alpha\mu_{l} + (1 - \alpha)\mu_{\mathrm{g}}. \tag{17}$$

The normal forces acting on the liquid surface ($\boldsymbol{F}_{\mathrm{s}}$) is given by the sum of the Laplace pressure and the DJP:

$$\boldsymbol{F}_{\mathrm{s}} = (\sigma\kappa(x) + \Pi)\boldsymbol{n}, \tag{18}$$

where $\kappa(x) = \nabla \cdot \boldsymbol{n}$ and $\boldsymbol{n} = \nabla\alpha/|\nabla\alpha|$ are the curvature of the interface and the unit vector normal to the interface, respectively. Since the fluid type remains constant along particle paths and using the continuity equation, α is passively advected by

$$\frac{\partial\alpha}{\partial t} + \nabla \cdot (\boldsymbol{U}\alpha) = 0. \tag{19}$$

Based on the updated void fraction field, the fluid properties (equations (16) and (17)) and the normal force (equation (18)) are calculated and the interface is reconstructed. Although equations are written for convection of phase fraction, there can be always the possibility of getting false diffusion [25]. A possible remedy used in OpenFOAM is introducing an extra term called artificial compression to the equation of phase fraction convection. Physically its role is exerting a pressure on the interface to keep it from dispersing and get a sharp interface. In this manner, the transport equation becomes [26]

$$\frac{\partial\alpha}{\partial t} + \nabla \cdot (\alpha\boldsymbol{U}) + \nabla \cdot (\alpha(1 - \alpha)\boldsymbol{U}_r) = 0, \tag{20}$$

where $\boldsymbol{U}_r = \min[C_r\boldsymbol{U}, \max(|\boldsymbol{U}|)](\nabla\alpha/|\nabla\alpha|)$ is a liquid velocity relative to gas velocity and is normal to the interface

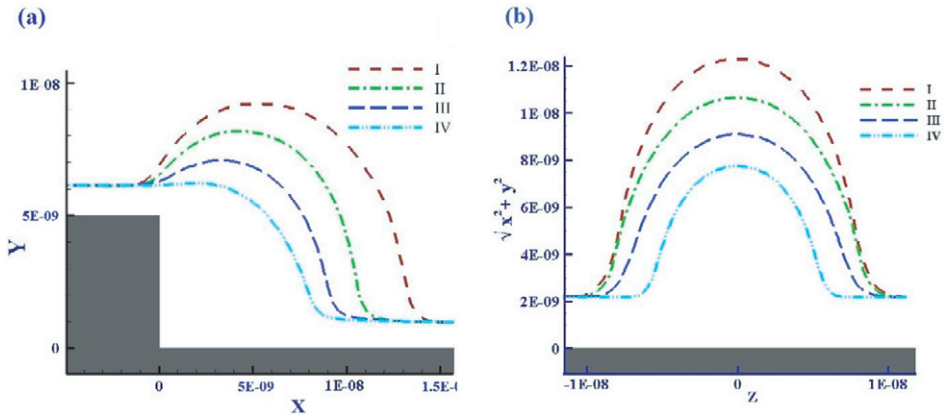

Figure 7. By decreasing volume of the droplets the right-hand side contact lines move toward the wedge more than the left-hand side ones. The volumes are $V_{\mathrm{I}} = 3200\,\mathrm{nm}^3, V_{\mathrm{II}} = 2500\,\mathrm{nm}^3, V_{\mathrm{III}} = 1800\,\mathrm{nm}^3$ and $V_{\mathrm{IV}} = 1000\,\mathrm{nm}^3$. In all the cases the DJP corresponds to the minus case with $B = 0$ and $C = 3.8$. The parts (a) and (b) display $z = 0$ and $x = y$ planes (see part (b) of figure 5).

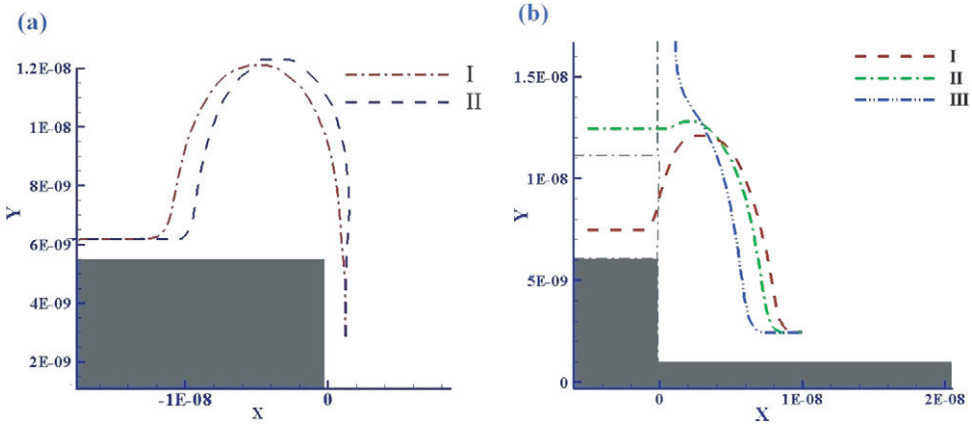

Figure 8. The effect of the step height on the dynamics of nanodroplets positioned on the top and the bottom sides of a step. In the part (a) dashed–dotted and dashed lines correspond to $h = 5$ and $h = 20$, respectively. All the profiles are shifted to the frame of the case with $h = 5$. Also in the part (b) the heights are $h_{\mathrm{I}} = 6$, $h_{\mathrm{II}} = 11$ and $h_{\mathrm{III}} = 20$. In all the case the DJP parameters are $B = 0$ and $C = 3.8$.

that applies the artificial compression on the surface. For the constant C_r that adjust compression, value in $[1, 4]$ is recommended so that ensure a sharp interface and limit α to values between 0 and 1 [27]. Multidimensional universal limiter with explicit solution (MULES) is used for solving equation (20). Based on the the term $\alpha(1-\alpha)\boldsymbol{U}_r$, the region under the influence of compression velocity has phase fraction values other than 0 and 1.

The governing equations were discretized by the finite volume method (FVM) with a collocated grid arrangement and the InterFoam solver of the OpenFOAM CFD package was employed to solve the equations. The solver was extended to include the effect of the DJP force. Detailed descriptions of the InterFoam can be found in [28]. The domain was modelled and meshed with the blockMesh OpenFOAM utility. A cubic box as a simulation domain was considered. For the gas interface (atmosphere) an open boundary condition was considered and for the sides a simple zero gradient wall boundary conditions was applied for all the variables. For visualization of results the interface was considered to be the places where $\alpha = 0.5$. The solution procedure is summarized in the following [29]:

- Generate mesh and set the boundary conditions for all the fields.

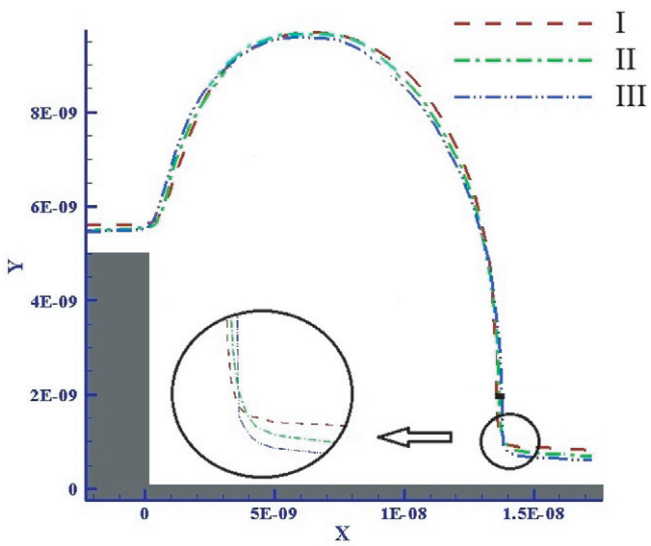

Figure 9. The stationary shapes of the droplets for the plus cases. The disjoining pressure values correspond to I ($B = -4$, $C = 1.3$), II ($B = -6$, $C = 0.4$) and III ($B = -10$, $C = 0.2$).

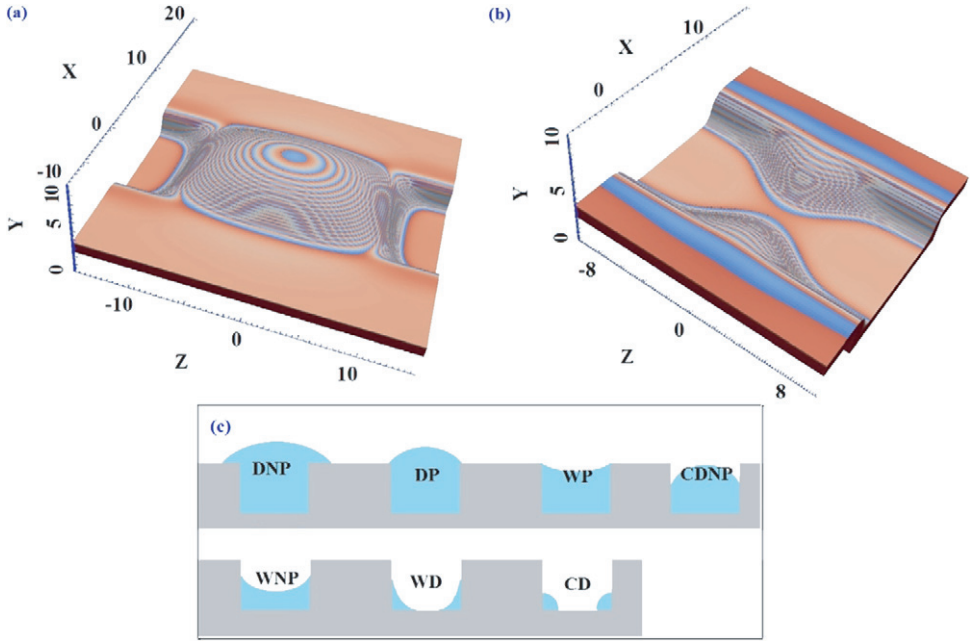

Figure 10. (*a*), (*b*) The simulation results for the morphology of droplets positioned on a groove for the minus case of the DJP. (*a*) The droplet is pinned at the edge of the groove. (*b*) The droplet is broken down into two droplets, which settle in the corners. The disjoining pressure parameters in the both cases are $B = 0$ and $C = 3.8$. (*c*) Different morphologies that can be found in a typical groove by changing the liquid volume. For definitions see the text.

- Read the material properties and the DJP.
- Adjust time step according to the courant number.
- Solve α equation (equation (20)).
- Calculate local density ρ and the dynamic viscosity μ from equations (16) and (17).
- Solve momentum equation (equation (15)) with PISO algorithm and Rhie and Chow interpolation.

The numerical algorithm was verified by comparing the results with those of the boundary integral method [15]. In the case shown in figure 4 the step height is equal to 5 and the DJP profile is the plus case with the parameters $B = -2.5$ and $C = 6$, corresponding to $\theta_{eq} = 114.7^{\circ}$. Also, the area of the droplet is equal to 250. As can be seen the results are in very good agreement with boundary integral outcomes.

3. Results and discussion

In the following we discuss the equilibrium wetting morphologies that can be found in the considered topographies, namely, in the edges, the wedges, the steps and the grooves. In all the considered cases, except the cases where we study the effects of the DJP, the applied DJP corresponds to the minus case with $B = 0$ and $C = 3.8$, which yields $\theta_{\mathrm{eq}} = 115^{\circ}$. By changing the control parameters such as the DJP, the liquid volume and the type of the topography, different configurations can be found. In the steps, the droplets that are positioned on the top side of the step incline to move towards the edge and get pinned as depicted in figure 5. Also, the droplets very near to the wedge area of the step move inside the wedge area. In both the cases the droplets cannot move to another side of the edge and for displacing the droplets an external force is required to overcome the energy barrier. The effects of the factors such as the type of the DJP, geometries and volume of the droplets located near the step are illustrated in the typical planes shown in figure 5.

As explained, wetting at the nanoscale is different from that understood at the micro- or larger scales. Equations (8) and (13) indicate that the equilibrium contact angle can be adjusted by dimensionless parameter B and C in the DJP expression. Figure 6 shows that varying parameter C affects the final shape of the droplets and increasing this parameter from $C = 1.5$ to $C = 3.5$ in the minus case with $B = 0$, which correspond to $y_0 = 1$, results in further motion of the right side contact line towards the wedge area while the left contact line does not experience any considerable change. Similarly, when the volume of the droplets increase, as shown in figure 7, in contrast to the contact line near the edge of step, which does not experience remarkable changes, the other contact line exhibits appreciable changes.

The geometrical parameters are other factors that affect the morphology of the droplets and the height is the only geometric parameter for the step where based on its size the stationary shape of droplets changes. Figure 8 illustrates that any increase in the height of the step results in further motion of the contact line of the droplets toward the edge, if the droplet is placed on the top side of the step. If the droplets are positioned on the bottom side of the step, they move further to the wedge area of the step.

All the cases investigated so far belong to the minus case of the DJP. Changing the type of the DJP from the minus to the plus one can change the morphology, as shown in figure 9. As is evident from figure 9 thin-film thicknesses for different values of B change. For example, for the DJP corresponding to I ($B = -4, C = 1.3$), II ($B = -6, C = 0.4$) and III ($B = -10, C = 0.2$), the film thicknesses are $y_0 = 0.629$,

$y_0 = 0.67$ and $y_0 = 0.79$, respectively. For the droplets on the top side of the step the situation is appreciably different. For the minus case the droplets find their stationary profiles near the edges or the tip area, while for the plus case the droplets on the top sides are formed on the positions very far from the edges or the tip, namely, the places where the droplets do not feel any change in the DJP ($d\Pi = 0$).

Different morphologies which can be controlled by the DJP, volume and geometries can emerge in the grooves and all these morphologies for small volume of the liquids are shown in figure 10. In the absence of the wedge (height equal to zero) one can see two morphologies: droplet for strong values of the DJP and partial wetting for weak values. When a small volume of a liquid is positioned in a groove, it is divided into two portions and depending on the DJP can form a droplet in the corner (CD) or with a minus curvature is settled in the wedge area (WD). By increasing volume of the liquid other morphologies, namely, DNP (droplet non-pinned), DP (droplet pinned), WP (wedge pinned), CNDP (corner droplet non-pinned), wedge non-pinned (WNP) will appear as shown in figure 10. Very large droplets get pinned at the edges of the groove. Changing the size of the channel yields different morphologies. Figure 11 displays the morphology diagram for two widths of the channel. As can be observed from the diagram by decreasing width of the channel, which results in increasing volume ratio of the liquid to the empty space of the channel, droplet breaking is reduced and the phase diagram switches to the right. On the other hand, the ratio of the liquid volume to the empty space of the channel in constant disjoining pressure specifies the type of morphology. For more complex geometries in this research, stable or metastable regions over the edge and wedge are found. Droplets residing near these hetergeneities of solid substrates exhibit a disjoining pressure dynamics which is obvious from the DJP. By increasing the complexity of the geometry the number of morphologies that can be observed will increase. Similar to the previous topographical elements, in any other geometry the droplets get pinned at the edges and settle in the wedges. Figure 12 shows different regions of the edges at which droplets may rest. As shown in this figure the droplets situated in one side of the edge incline to be at that side and gets pinned at the edges of that side. Also, according to figure 12, if a droplet is positioned in front of the edge symmetrically, it can move to the left or the right side of the edge. The most unstable situation of the droplets is when the droplets are at the tip of the edge as depicted in part (c) of the figure. In this situation the droplet will move towards the top side of the edge and will remain adjacent to the tip for the minus form of the DJP. For the plus form of the DJP the same behaviour is observed but the droplet moves away from the tip region. However, for the wedges, the droplets positioned in front of the wedge start to move into the wedge area and after some relaxations stay there.

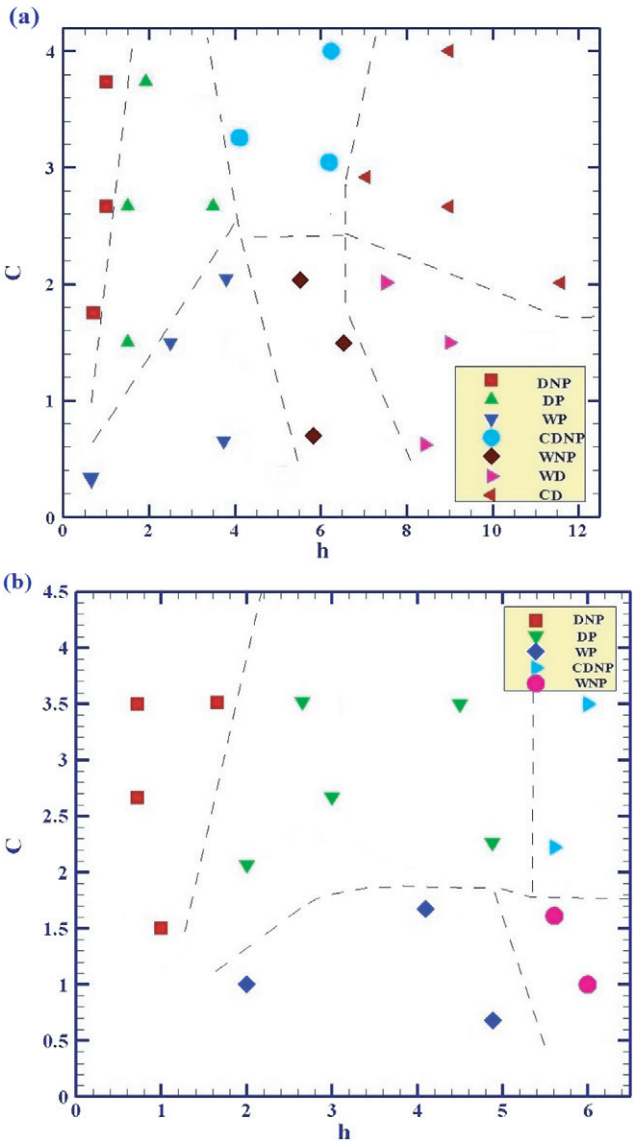

Figure 11. Morphology diagram in the groove for the width 12.5 (*a*) and 6 (*b*). All the results are obtained for the minuse case of the disjoining pressure with $B = 0$ and $C = 3.8$. For definitions see the text.

4. Conclusion

In summary, we calculated the distribution of the intermolecular forces or the disjoining pressure over several basic nanostructures considering Lennard–Jones type pair potential interactions between the atoms. The DJP for the step can be calculated analytically but for the three-dimensional edges and wedges the procedure was conducted numerically. For any of these structures the DJP can take various forms depending on the materials of the substrate, the liquid and the coating layer on the substrate. Two major forms, namely the plus and the minus forms were identified. Different dimensionless parameters that can be adjusted to obtain an equilibrium contact angle were introduced.

Using the derived disjoining pressure and based on the VOF hydrodynamic calculations, the local minimum energy regions were determined and a variety of morphologies, according to these states, were specified. The effects of different parameters such as the geometrical parameters, volume of the liquid and type of the disjoining pressure on the morphologies were reported.

For a step it was found that when the droplets are positioned on the top side of the step they remain near the

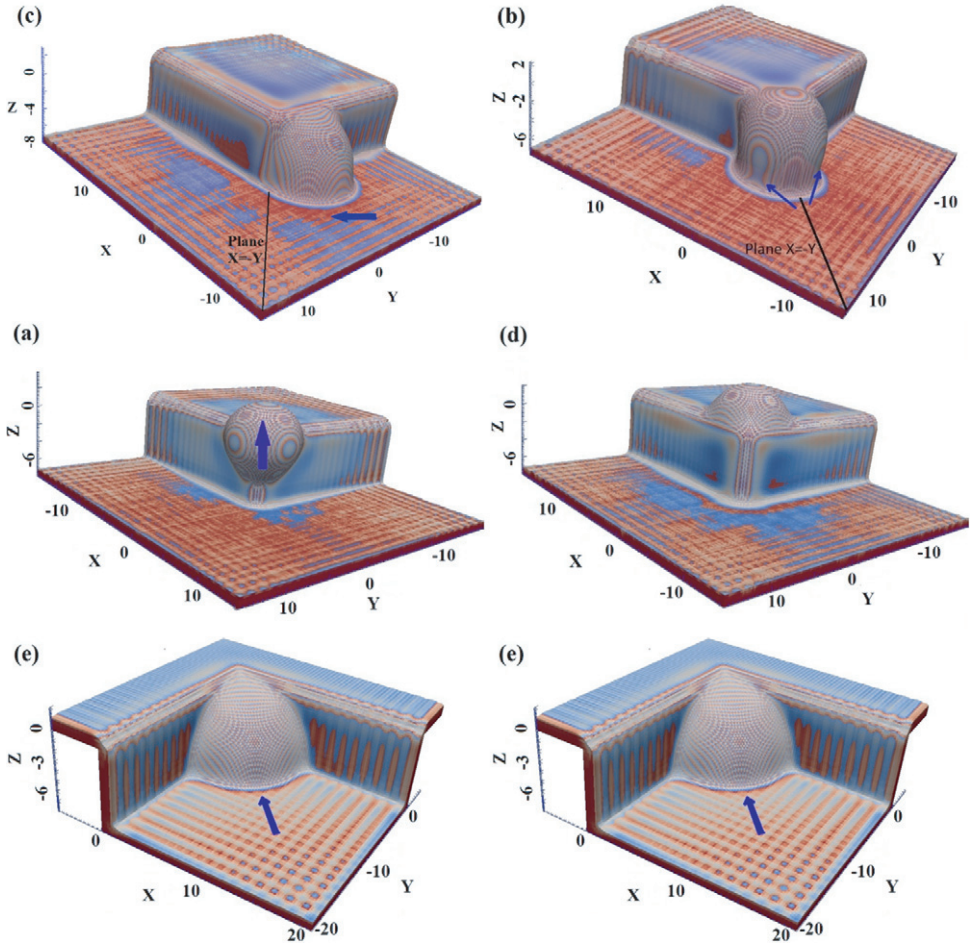

Figure 12. The final positions and shapes of droplets that initially situated in different positions. Direction of arrows shows the direction of droplets motion. (*a*) A droplet that is initially situated symmetrically in front of an edge. (*b*) The droplet of part (*a*) has moved to the right side. (*c*) A droplet which is positioned at the tip of the edge. (*d*) The droplet in part (*c*) has moved to top side. (*e*) The final situation of a droplet positioned near the wedge region. (*e*) The final state of a droplet the is positioned near the tip area. The results belong to the minus form of the DJP.

edges for the minus case of the DJP and are formed at positions very far from the edges for the plus case of the DJP. Also, the droplets near the wedge settle in the wedge area for both the DJP cases. For an edge it was found that the droplets are not stable at the tip and move to the sides and depending on the type of the DJP the droplets will stay near or far from the tip area. If a droplet is considered in front of an edge it is moved to one side.

It is revealed that for a groove the liquid volume can have substantial effect on the observed morphology. For small volumes the observed shapes are the corner droplets (CD) and the wedge droplets (WD). By gradually increasing the volume of the droplets, other configurations such as the wedge non-pinned liquids (WNP), corner droplets non-pinned (CDNP), wedge pinned liquid, droplet pinned and droplet non-pinned gradually appear.

Our results can be useful in understanding the behaviour of systems containing nanodroplets. For example, most of the giant fields produce hydrocarbons from carbonate reservoirs. The studies have revealed the importance of taking into account nanoscale pores in studying or modelling carbonates [30]. As already stated, the results can also be used in handling, controlling and guiding liquids in emerging nanofluidic devices.

References

[1] Indekeu J O 1995 *Acta Phys. Pol.* D **26** 1065–100
[2] De Gennes P G, Brochard-Wyart F and Quéré D 2003 *Capillarity and Wetting Phenomena: Drops, Bubbles, Pearls, Waves* (New York: Springer)
[3] Dietrich S 1999 *New Approaches to Old and New Problems in Liquid State Theory* (*NATO-ASI Series C* vol C529) ed C Caccamo *et al* (Dordrecht: Kluwer) pp 197–244
[4] Bauer C and Dietrich S 1999 *Phys. Rev.* E **60** 6919–41
[5] Karniadakis G E, Beşkö A and Aluru N R 2005 *Microflows and Nanoflows: Fundamentals and Simulation* (New York: Springer)
[6] Rauscher M and Dietrich S 2008 *Annu. Rev. Mater. Res.* **38** 143–72
[7] Oliveira N M, Neto A I, Song W and Mano J F 2010 *Appl. Phys. Express.* **3** 085205
[8] Brinkmann M and Blossey R 2004 *Eur. Phys. J.* E **14** 79–89
[9] Lipowsky R, Lenz P and Swain P S 2000 *Colloids Surf.* A **161** 3
[10] Seemann R, Herminghaus S and Jacobs K 2001 *Phys. Rev. Lett.* **87** 196101

[11] Seemann R, Brinkmann M, Kramer E J, Lange F and Lipowsky R 2005 *Proc. Natl. Acad. Sci. USA* **102** 1848–52
[12] Seemann R, Brinkmann M, Herminghaus S, Khare K, Law B M, McBride S and Michler D 2011 *J. Phys.: Condens. Matter* **23** 184108
[13] Herminghaus S, Brinkmann M, Seemann R 2008 *Annu. Rev. Mater. Res.* **38** 101–21
[14] Moosavi A, Rauscher M and Dietrich S 2006 *Phys. Rev. Lett.* **97** 236101
[15] Moosavi A, Rauscher M and Dietrich S 2009 *J. Phys.: Condens. Matter* **21** 464120
[16] Rath S, Heilig M and Port H 2007 *Nano Lett.* **7** 3845–8
[17] De Gennes P G 1985 *Rev. Mod. Phys.* **57** 827–63
[18] Derjaguin B V 1940 *Zh. Fiz. Khim.* **14** 137–47
[19] Kundu S, Ganesan R, Gaur N, Saifullah M S M, Hussain H, Yang H and Bhatia C S 2012 *Sci. Rep.* **2** 617
[20] Getta T and Dietrich S 1998 *Phys. Rev.* E **57** 655–71
[21] Tsekov R and Toshev B V 2012 *Colloid J.* **74** 266–8
[22] Grün G, Mecke K and Rauscher M 2006 *J. Stat. Phys.* **122** 1261–91
[23] Netz R R and Andelman D 1997 *Phys. Rev.* E **55** 687–700
[24] Hirt C W and Nichols B D 1981 *J. Comput. Phys.* **39** 201–25
[25] Versteeg H K and Malalasekera W 2007 *An Introduction to Computational Fluid Dynamics: The Finite Volume Method* (New York: Pearson Education)
[26] Rusche H 2002 Computational fluid dynamics of dispersed two-phase flows at high phase fractions *Thesis* Imperial College, London
[27] Wörner M 2012 *Microfluid. Nanofluid.* **12** 841–86
[28] Roisman I V, Weickgenannt C M, Lembach A N and Tropea C 2010 *23rd Annual Conf. on Liquid Atomization and Spray Systems (Brno, Czech Republic, September)*
[29] Issa R I 1986 *J. Comput. Phys.* **62** 40–65
[30] Biswal B, Ren P, Held R J, Bakke S and Hilfer R 2007 *Phys. Rev.* E **75** 061303